BIRD-STRIKE DAMAGE TOLERANCE ANALYSIS OF COMPOSITE TURBOFAN ENGINES

Anthony Zammit, Minki Kim and Javid Bayandor
The Sir Lawrence Wackett Aerospace Centre
School of Aerospace, Mechanical and Manufacturing Engineering
Royal Melbourne Institute of Technology Melbourne, Victoria, 3001

Keywords: **Bird-strike, Damage Tolerance, Propulsion, Fan Blades, Advanced Composites**

Abstract

This paper details and discusses numerical methods of simulating bird-strikes onto metallic blades and full fan, and onto a composite blade, using Smoothed Particle Hydrodynamics (SPH) and Arbitrary Lagrangian Eulerian (ALE) method to model the bird. Stronger emphasis is put on the SPH technique. The metallic models were used to investigate modelling issues and investigate the appropriateness of the fluid-structure interactions. Furthermore a methodology has been developed for analysing impact onto an advanced composite blade for both SPH and ALE techniques.

1 Introduction

Engines are subject to Foreign Object Impact (FOI), including bird-strikes. Unlike metals, advanced composites, that are becoming part of new generation propulsion systems, can sustain invisible internal damage consisting of delamination, fibre fracture, and/or matrix cracking. During a bird-strike, the fluid-solid interaction created by the phase change of the bird causes the composite blade to experience complex through-thickness loading. The worst case scenarios include blade break-offs, leading to catastrophic events; possibly involving severe damage to nearby aircraft structures, other engine components, payload and even injury or death sustained by crew members.

Bird impact is initially a solid-structure interaction problem. When a bird perpendicularly impacts a solid, rigid target, a large pressure shockwave is created in the bird medium. This wave propagates through the bird, instantly breaking its internal bonds, causing a phase change to fluid; thus changing the analysis to a solid to fluid interaction problem. Material at the edge of the bird suffers a sharp pressure gradient and is therefore radially forced outwards, causing the impact area to grow. The relative speeds of bird impact on a fan cause the generated shockwave to propagate in the opposite direction to the impact. As the shockwave propagates through the bird medium, 'release' waves propagate faster and eventually catch and dissipate the shockwave. Once this has occurred, the bird material acts as a subsonic fluid and exerts a lower pressure, until the last part of the bird reaches the target, at which point the pressure decays to zero. The compression of bird material during the impact causes a change in bird density, which is non-linearly related to the pressure induced on the target. However, this soft body impact on a dynamic, loaded and deformable blade with complex geometry is currently not fully understood.

Through this work it has been aimed to capture this intricate, complex, non-linear behaviour of the fluid-structure interaction of the bird-strike onto the fan. In addition it has been attempted to predict the damage sustained, using the mesh free particle technique, Smoothed Particle Hydrodynamics (SPH). In order to achieve this, the usual aerodynamic and centrifugal loads must be considered. These loads can vary as each blade is deformed by the impact thus further complicating the situation. The loss or deformation of blade material shifts the centre of gravity about the centre of rotation potentially causing undesirable vibrations which must be analysed. Furthermore, it is desirable to track each piece of debris to ensure that its

consequential damage to later engine stages does not render the engine unsafe.

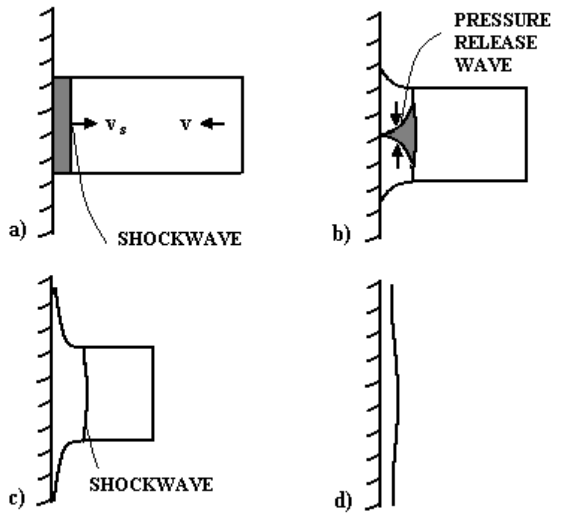

Fig. 1. Four phases of normal impact onto a rigid target. The shaded regions represent extremely high pressures

2 Bird Impact Theory

Bird impact is a fluid-solid interaction problem for velocities over 50m/s. This differs from a rigid solid-solid interaction in that momentum of the impactor is transferred to the target progressively. Four phases of impact as shown in Fig. 1 have been suggested [1]. For simplicity, the following theory assumes that the bird is cylindrical and impacts on a perfectly rigid plate.

The impact consists of four stages. Stage a) occurs at the moment of impact. During this stage, the material is suddenly decelerated to a stop, initiating a shockwave in the material at the point of impact, known as the Hugoniot shock pressure as depicted in Fig. 1a, with the magnitude of:

$$P_H = \rho_0 v_s v \quad (1)$$

Where ρ_0, v_s and v are the density of the bird, speed of the shock and impact speed of the bird, respectively.

During Stage b), as the pressure gradient around the edge of the cylinder becomes very high, the material is forced out radially and is referred to as released. As this occurs, the shockwave propagates up through the bird in Fig. 1b. Radial release waves move inward radially and eventually catch up to the shocked material, causing the shockwave to dissipate and the pressure at the target face to decay until a steady flow is occurs as shown in Fig. 1c.

This steady state pressure P_S is shown in Eq.(2)

$$P_S = k\rho_0 v^2 \quad (2)$$

where k is 0.5 for an incompressible fluid. However, complimentary studies have shown that this value approaches 1.0 for a bird [2]. As the end of the bird approaches the target, the pressure decays down to zero [1]

In practical fan blade applications, this behaviour does occur, however, as the impact surface is deformable and intricately curved in three dimensions, and the bird impactor is not cylindrical, the impact behaviour is far more complex. The impact shock and release can travel in multiple directions. In addition, the angle of attack of the bird compared to the blade plays a role in the severity of the impact with zero angle of attack causing barely any damage and 90^0 receiving maximum [3].

3 Mathematical Representation of the Bird

It was necessary to define an equation of state for the bird, which relates the pressure experienced by the particles to volume. The linear polynomial is a simple yet suitable model for a bird [4] and is shown below:

$$P = C_0 + C_1\mu + C_2\mu^2 + C_3\mu^3 + (C_4 + C_5\mu + \quad (3)$$

Where C_x are constants and

$$\mu = \frac{\rho}{\rho_0} - 1$$

All C values were set to zero except for C_1 which represents the bulk modulus of the bird material. ρ is the density of the bird between the target and the shockwave

3.1 Smoothed Particle Hydrodynamics (SPH)

The bird has been modelled using Smoothed Particle Hydrodynamics (SPH). SPH involves

the motion of a set of points. At any time, the velocity and thermal energy of these points are known. Each point is assigned a mass and radius and hence are referred to as particles [5]. The use of particles has the advantage over element based methods in that it is free from element distortions.

For any given particle, the fluid forces exerted on it are dependent on the mass of surrounding particles and interpolation or kernel function. The higher the mass of a surrounding particle, the more influence it exerts on a given particle. The kernel function determines the amount influence the surrounding particles exert, with the closest particles exerting the most influence. Therefore, the amount of force exerted between particles can be thought of as a gravity [2]. Thus particles must be spaced as evenly as possible.

The kernel function used was a centrally peaked cubic B-spline shown in Fig. 2

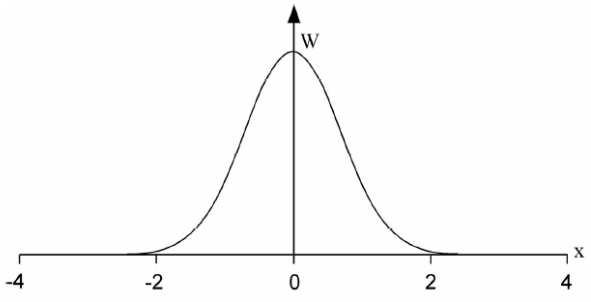

Fig. 2. The cubic B-spline

3.2 Arbitrary Lagrangian-Eulerian (ALE)

Pure Lagrangian and Eulerian methods contain shortcomings in fluid dynamic applications, such as bird-strikes. The Lagrangian method often suffers from high element distortion, resulting in less accuracy. The Eulerian method is computationally expensive as the void part is fixed in the space.

To overcome these drawbacks Arbitrary Lagrangian-Eulerian method (ALE) is recommended [11], [12] for bird-strike applications. As its name implies, ALE combines the short computational time of the Lagrangian technique with the ability to derive accurate results under high deformation of the Eulerian technique

The void part in ALE is capable of moving together with the material mesh and if necessary, it could be stretched and expanded laterally while contracting longitudinally (Fig. 3). With these notable benefits, a larger number of elements can be eliminated in ALE method, and the computational time can be significantly reduced [6]

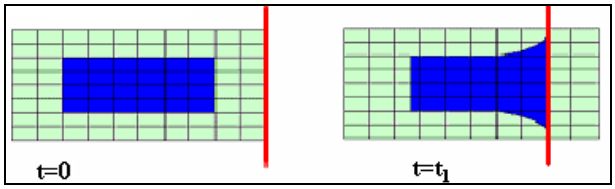

Fig. 3. Simplified ALE mesh movement; void (green colour), material mesh (blue colour) [7]

3.3 Calibration of Methods

SPH and ALE techniques were used as comparisons due to the limited availability of experimental data. In order to compare, the bird models needed to be calibrated to match each other as closely as possible. Results are shown in Fig. 4 below. Velocities of 116, 197, 253 and 300m/s were tested with 300m/s showing the greatest variation. Although resultant velocities are higher in bird-to-blade impact, the velocities perpendicular to the surface of the blade will be around this mark. Force-Time histories were adopted because they were more easily attained due to the growing impact area [2].

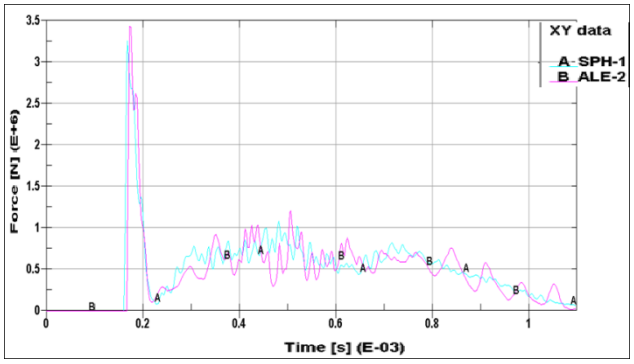

Fig. 4. SPH vs ALE force-time histories for a perpendicular impact of 300m/s on a rigid plate.

Early SPH parametric studies [8] revealed that it was necessary to reduce the Time-Step Scale Factor (TSSFAC) from the default of 0.9 to 0.45 in order to prevent penetration of SPH particles through the target material.

The SPH parameters were kept at the default LS-Dyna values. The smoothing length scaling factor was set to 1.2 and the smoothing length was determined from the divergence of velocity.

As ALE approach, a comparison of mesh density was conducted with different number of elements representing void and bird part. It was found that a moderately fine mesh model gave the closest correlation with theoretical values when the bird was travelling within the range of 116-300 *m/s*. In this study 69696 numbers of elements for the bird was used. The materials used for the void part were air or vacuum. It was observed that setting the ratio of surrounding void volume to bird part volume of 4.7 derived the most stable plots. If a smaller ratio was selected, more instability was observed since the void could not continue to encompass the entire expended bird parts during impact.

4 Method

4.1 Single Blades

The blade models consisted of one blade of shells connected to solid rigid elements. The models contained impact, centrifugal as well as aerodynamic loading. Centrifugal loading was achieved by assuming the global axis rotates with the blade and thus the rigid hub was able to be restrained in all degrees of freedom. Bird impact occurred at 250mm of the span, perpendicular to the radius of the blade. The impact velocity was the resultant vector of the bird travelling at 103m/s perpendicularly impacting the blade of linear velocity of 420m/s

A simplistic method was adopted for including aerodynamic loading. The following assumptions were made in this analysis:

- Lift, drag and torque act only from the aerodynamic centre which was assumed to be 22.2% chord therefore C_{M0} is constant along the span
- Strip theory applies
- The lift curve slope is infinitely linear
- The velocity of the flow was taken as $v_{air} = 250$m/s and does not vary from root to tip
- The flow is perpendicular to the plane of the fan i.e., air flows in the negative z-direction
- The aerodynamic loads remain at the point of bird impact as impact occurs
- The aerodynamic loads remain unchanged in magnitude and direction, even when the blade is deformed.
- Extension of the blade due to centrifugal loading is negligible, and therefore r is the distance from the centre of rotation to a point on the undeformed blade
- There is no aerodynamic twist in the blade; ie, the lift curve slope C_{L_α} is constant along the span
- For the composite models, the loads disappeared after the nodes they were applied to, were deleted.

The blade was divided into four strips with lift, drag and torque loads along roughly 22.2% of the blade chord (representing the aerodynamic centre). The more strips that are taken, the more accurate the analysis will be; with the limit being the length of the elements. The loads were applied directly to the nodes (1 node per strip). The area and angle of each strip to the direction of rotation were measured at three points along the span and approximated as quadratic functions.

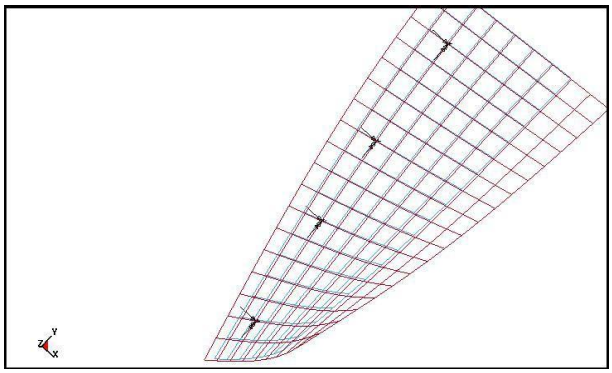

Fig. 5. The positions of the aerodynamic loads are depicted by the black arrows.

An elemental strip of area, S(r) is theoretically c(r)×dr. The chord, c(r) was measured as the linear distance from the leading edge node to the trailing edge node of the same row of shells. ‘dr’ was measured as the length of the shell on the leading edge. The angle of incidence i(r) was measured relative to the plane

of rotation. The distance r from the centre of rotation was measured up until dr/2. The chord, area and angle of incidence as a function of radius were found to be as shown below:

$$c(r) = -0.0016r^2 + 0.35r + 4.69 \quad (4)$$

$$S(r) = 0.0013r^2 + 2.22r + 1184.84 \quad (5)$$

$$i(r) = 2.43 \times 10^{-6}r^2 - 0.0046r + 2.30 \quad (6)$$

As four strips were taken, the area of the elemental strips in each quadrant must be summed to make the area of the quadrant. The classical aerodynamic equations were used:

$$L = \frac{1}{2}\rho_{air} v_R^2 S(r) C_L(r) \quad (7)$$

$$D = \frac{1}{2}\rho_{air} v_R^2 S(r)(C_{D0} + kC_L(r)^2) \quad (8)$$

$$T = \frac{1}{2}\rho_{air} v_R^2 S(r) C_{M0} c(r) \quad (9)$$

ρ is the density of air taken to be $1.225 \times 10^{-6} g/m$ is the relative velocity of the flow and the blade. The blade linear velocity is $v_b =$, therefore, the relative velocity is $v_R^2 = {v_{air}}^2 + \omega^2$. The rotational speed was taken as $\omega = 0.7645\ rad/$ (7300RPM). The surface area is shown in eq.(5). C_L was taken to be $C_L = C_l$ where $C_{L_\alpha} = 4.3\ 1/$ and $\alpha = (i(r) - \mathrm{Tan}^{-1}(v_{air}/\omega.$ (was taken to be 0.001. k was 0.15, assuming that e=0.9 and the aspect ratio was found to be blade length divided by average chord, which was 2.34. was taken as -0.01.

In order to split the loads into components, the following transformations were used (refer to Fig. 6 for the coordinate system).

$$\begin{bmatrix} X \\ Z \end{bmatrix} = \begin{bmatrix} sin\theta & cos\theta \\ cos\theta & -sin\theta \end{bmatrix} \begin{bmatrix} L \\ D \end{bmatrix} \quad (10)$$

Where

$$sin\theta = \frac{v_{air}}{v_R} = \frac{v_{air}}{\sqrt{v_{air}^2 + (\omega r)^2}} \quad (11)$$

$$cos\theta = \frac{v_b}{v_R} = \frac{\omega r}{\sqrt{v_{air}^2 + (\omega r)^2}} \quad (12)$$

and θ is the angle between the velocity vectors and the blade rotation occurred about the z-axis

Torque was simply applied in the y direction.

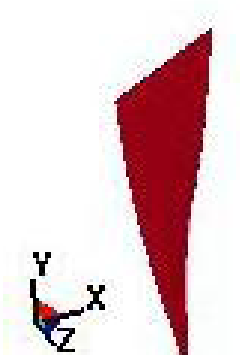

Fig. 6. The coordinate system used.

4.1.1 Metallic Blades

The metal used was TIMETAL® 6-4 Titanium Alloy (Ti-6Al-4V; ASTM Grade 5). It was modelled taking plasticity into consideration. The material properties are shown in Table 1.

Table 1. Titanium alloy material properties

Yield Stress	980MPa
Young's Modulus	112500MPa
Density	0.00442g/mm^3
Poisson's ratio	0.31

The dynamic relaxation method [9] was used to initialize the centrifugal loads. Dynamic relaxation is a quasistatic method that attempts to prestress a structure. A Dynamic Relaxation Factor (DRFCTR) must be defined, which is $1 - c \times$ where c is damping coefficient at time dt. When the ratio of current kinetic energy to maximum kinetic energy (excluding rigid body modes) reduces to DRTOL, the dynamic relaxation phase ends. In this analysis, DRTOL=0.001 and DRFCTR=0.995 However, a linear ramp-up method was used to initialize the aerodynamic loads over 25ms.

As suggested by ref [10], the Flanagan-Belytschko viscous hourglass control was used as the control solution and was compared to fully integrated shell solution.

4.1.2 Composite Blades

The composite used was AS4 carbon fibre composite. The Chang-Chang failure criteria was utilized

Eight plies were assumed with the following orientations in degrees: [90, 90, 45, -45, 45, -45, 90, 90] measured from the positive

x-axis (refer to Fig. 6 for the reference axis). Each ply was modelled as an integration point of a shell. Since only one shell layer was used, delamination was neglected in this analysis.

The composite analysis was conducted in two phases. The first was to initialize the aerodynamic and centrifugal loading and the other was the impact analysis.

A linear speed ramp-up method [10] was used to initialize the centrifugal and aerodynamic loads. The ramp up was for 75ms. If the ramp up is too sudden, the failure criteria of the material will be met too soon and high oscillatory modes will be excited. In contrast, if the ramp up is too slow, the computational cost will be high. In addition, if under integrated shells are used, long ramp ups encourage hour-glassing modes to dominate.

At the end of the first phase, the analysis was stopped and the bird model was added to the input file along with its velocity. In addition, to eliminate slight oscillations in the blade, the blade node's velocity was set to zero. Furthermore a "stress initialization" command was required to initiate the stresses and displacements of the blade from the first phase. A "restart analysis" commenced the second phase of the analysis.

To account for the nature of composite materials, several other factors needed to be considered. Since the orientation of the shell is important, invariant node numbering was invoked. This forced the analysis to use element bisectors to determine the local element axis rather than two nodes. This made accounting for element rotations more accurate.

The Lobatto integration rule was used to assume that the outer integration points lay on the surface of the shell. Additionally, laminated shell theory was used to avoid the assumption of constant uniform shear stress through the shell thickness.

4.2 Full Fan

The fan was made up of 29 blades. Aerodynamic loads were excluded from this analysis as this is still work in progress. However, centrifugal loads were still incorporated. These loads were also initiated by dynamic relaxation using DRTOL=0.001 and DRFCTR=0.995 using a body load. However, this gravity loading was deactivated after the dynamic relaxation phase and replaced by an initial linear velocity to each node ($'node = \omega \times r$) and a prescribed rotational motion to the rigid hub. The hub was restrained in all degrees of freedom except for its rotational axis. Damping relative to the hub was again employed as well as node-to-surface contacts for fluid-solid interaction. In addition, blade-to-blade contacts were employed using the slave segment-master segment configuration. In order to compare with the ALE results, blade contacts were omitted due to availability of ALE results and to avoid unnecessary sources of variation.

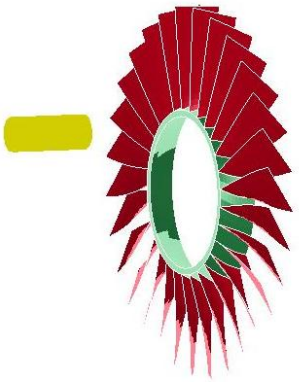

Fig. 7. Bird directed towards the fan

The different impact conditions shown in Table 2 have been compared

Table 2. The scenarios investigated. γ =the angle between the bird and the plane of rotation. All when $\gamma<90^0$ the bird has been angled into advancing blades. The angle of attack α was determined assuming the blade cross section is a straight line connecting the leading edge to the trailing edge.

γ (deg)	i (deg)	r (mm)	v_R (m/s)	α(deg)
90	65.7	300	251.4	41.6
90	49.4	400	322.7	30.8
90	35.8	500	395.9	20.7
75	35.8	500	420.8	22.1
60	35.8	500	442.8	24.2
45	35.8	500	460.9	26.7
90	35.8	500	471	0

5 Results and Discussion

In this section, the ALE technique has been compared to SPH and issues with modelling a full fan have been discussed.

5.1 Single Blade

5.1.1 Metallic Blade

It was attempted to initialize the aerodynamic loads along with the centrifugal loads using dynamic relaxation, however, the analysis was time consuming and the blade appeared unusually deformed. The weakness of the dynamic relaxation technique is that an appropriate dynamic relaxation factor needs to be chosen, otherwise the solution will not be accurate and it may not converge. This factor is found only by trial and error. As shell nodes contain rotational degrees of freedom, the dynamic relaxation method is less suited to shells than solids as the analysis time is longer.

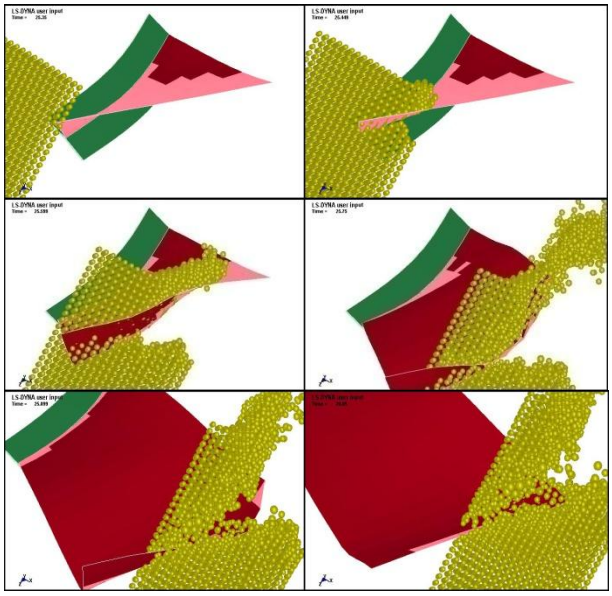

Fig. 8. Progressive impact of an SPH bird onto the metallic blade at times: 25.3 25.4 25.5 25.7 25.8 and 26 milliseconds viewed from above. The hourglass control method was the viscous Belytschko-Flanagan.

Fig. 8 shows the Fluid-Solid Interactions (FSI) between the blade and the SPH bird. The SPH material 'flows' appropriately. The bird impact in this case can be seen as a combination of yawed and oblique impact [11]. The contact pressure is not as high for these impacts as it is for a perpendicular impact; particularly when the angle of impact is below the "critical angle" (release waves form before the shockwave can propagate to the impactor side edge). Additionally, momentum is transferred into blade deformation, thus the change in impactor momentum is not as great compared to that on a rigid target. These effects are evident by comparing Fig. 4 and Fig. 9. The peak contact force for normal impact on a flat rigid target is in the order of 3.25MN, whereas the peak contact force on the fan reaches merely 0.5MN. The first diagram in Fig. 12 corresponds to a region of minimum contact force as shown in Fig. 9. The other two correspond to areas of maximum contact force. The pressure distribution appears to be fairly consistent over different peak force periods, thus the highest forces appear to the increased contact area. At 25.7ms, the bird is contacting on either side of the blade. The same behaviour can be observed when the SPH particle density is increased. A comparison between force-time histories is shown in Fig. 9.

The force time histories of the SPH and ALE techniques reveal the force time histories are quite similar in magnitude. The SPH technique appears to present more peaks than ALE, regardless of the mesh density. Integrating the curves gives a comparison of impact moment transferred. The control SPH model transferred a momentum of 99877Nms, the SPH model with eight times the mesh density transferred 114360Nms and the ALE model 132290Nms. Therefore, although the peak forces were higher for the SPH models, the ALE bird transferred far more impact momentum. This was evident visually as the blade looked more severely deformed.

After impact, the blade sprang back due to centrifugal stiffening in all cases.

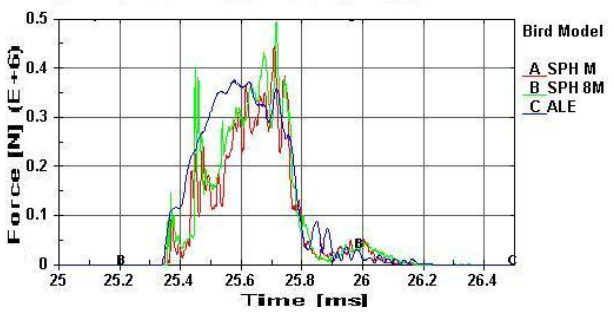

Fig. 9. Force time history comparison between SPH different particle densities (M represents the control density) and the ALE method from 25 *ms*

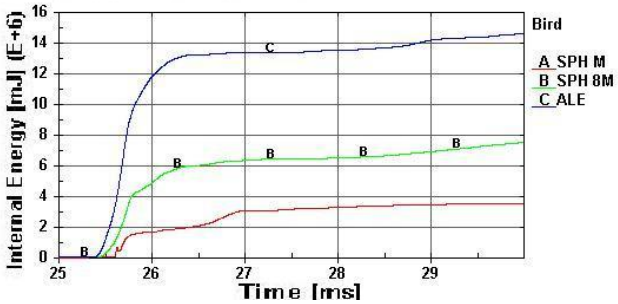

Fig. 10. Internal blade energy comparison between SPH different particle densities and the ALE method from 25 *ms.*

Fig. 10 shows the effects of the additional impact momentum. The internal energies are much higher for the ALE impact compared with the SPH impacts. Furthermore, the impact force and momentum between the two SPH solutions appears quite close, however, the internal energy was doubled when the mesh density was increased.

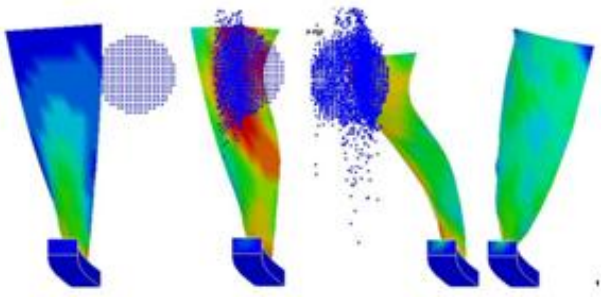

Fig. 11. Progressive Impact at 25.3, 25.6, 25.9, and 30 *ms* on the metallic blade.

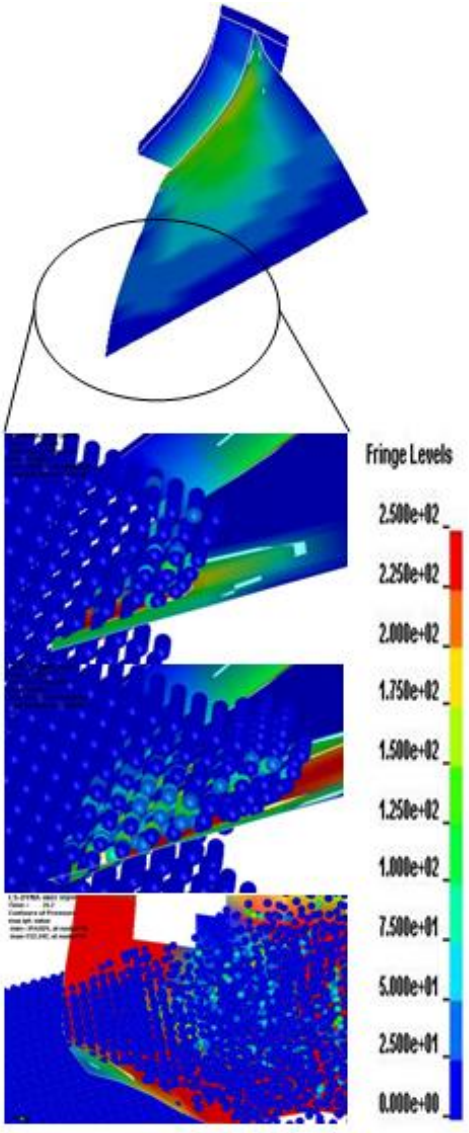

Fig. 12. Pressure plots for the SPH model impacting the metallic blade at times 25.4 25.45 and 25.7 milliseconds. Note in the bottom diagram, particles above the impact region have been blanked to show the pressured particles.

5.1.2 Composite Blades

The dynamic relaxation analysis did not provide converge for the composite blade therefore the restart analysis mentioned above was employed. In order for the restart analysis to work properly, it was necessary to use a fully integrated shell formulation. Attempts using the Belytschko-Tsay formulation resulted in high hour-glassing energies and a drop in global internal energy at the beginning of the second phase.

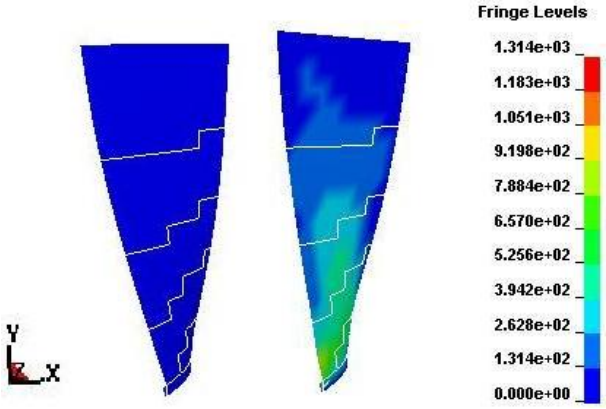

Fig. 13. A Von-Mises plot of the composite blade from phase 1, left undeformed (time=0) and right deformed (time=100ms). Units are in MPa

There are several advantages to the analysis undertaken. Performing the analysis in phases saved computational time by avoiding the use of SPH particles in the first phase. In addition, it may be possible to ramp up the blade more rapidly, with unrealistically high failure criteria for the first phase to avoid premature failure. This technique was used initially to study the effects of modifying the effective plastic strain, however it requires more research. Furthermore, the blade can be initialized using a TSSFAC of 0.9, which can be reduced to 0.45 for the subsequent impact analysis. As a bonus, this technique allows the user to modify minor parameters and restart the analysis from the impact phase rather than from the beginning.

In order to keep the composite from failing in the initialization phase, the effective failure strain had to be set to two percent from 0.436%. Despite this, catastrophic failure still occurred. Contrary to the metallic blade results, most damage appeared to occur at the point of impact rather than the root.

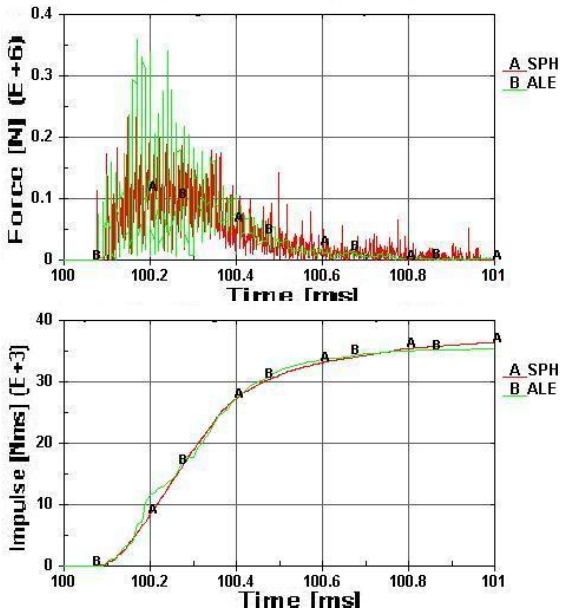

Fig. 14. Unfiltered force-time and impulse-time histories of the SPH and ALE models impacting the composite blade.

The force-time histories show that composite blades are far less tolerant to impact damage compared to metallic blades. Observation of the SPH and ALE force-time histories in Fig. 14 reveals that ALE varies more erratically within the first 0.4ms when compared to SPH, or ALE on the metallic models. However, on closer inspection, the peaks are more densely stacked for the case of the SPH solution. The ALE pattern is likely due to the fact that ALE represents a continuous medium. Thus it exhibits fewer peaks, and causes larger groups of composite elements to fail simultaneously, causing the large range of forces shown. The impulse time histories show close agreement thus showing the strength of both techniques.

It should also be noted that the pressures transferred to the blade were of similar magnitude. (Fig. 15) However, the pressure in the bird medium varied greatly between SPH and ALE. The pressure in the SPH particles was higher than that of the ALE elements. This is necessary due to the discrete nature of SPH.

The contact pressure plots in Fig. 15 show less pressure compared to impact on a titanium blade. This is due to failed elements being deleted. In addition, this provides less contact area lowering the overall contact force.

Fig. 16 shows crack propagation has been captured

Observation of matrix and fibre failure modes at each integration point reveal that the blade was damaged before impact. This could be due to the lack of integration points used. If one integration point which was used to represent many plies fails, then it is removed, along with all the integration points that it represented. Therefore, using few integration points gives an overestimate of the damage. Furthermore, using the Lobatto integration rule was used, thus assuming that the integration points laid on the surface of the shell. This would have caused a further conservative prediction of damage.

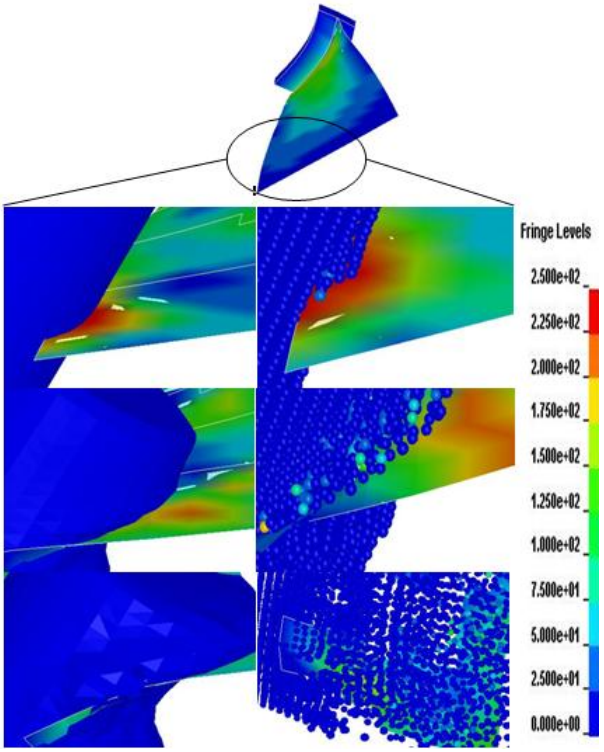

Fig. 15. Pressure plots in MPa for the ALE (left) and SPH (right) model impacting the composite blade at times 100.1 100.2 100.35 milliseconds. Note in the bottom SPH diagram, particles above the impact region have been blanked to show the pressured particles.

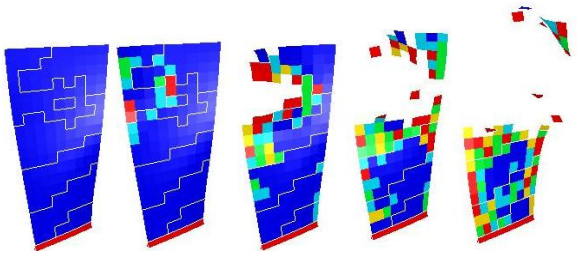

Fig. 16. Compressive matrix failure for the SPH model on the eighth integration point at 100.05 100.15 100.3 100.45 100.6 100.75 milliseconds blue=elastic red=failed (except at the hub).

5.2 Full Fan

In this section, the results of 0.9 TSSFAC have been compared to 0.45, in addition to contact definitions between blades. The models with no blade contacts have been included for the purpose of comparing with ALE results.

Three measures of damage have been employed; the number of blades damaged, maximum internal energy absorbed by the fan material and the maximum local energy per unit volume throughout the impact. The visual comparison of number of blades damaged is a simplistic approach, however, it is a good measure for the extent of damage and is the most practical when it comes to comparing with experimental results. The maximum internal energy numerically compares the overall severity of the impact and the maximum local internal energy is the best method of determining how close any part of the fan came to the maximum energy absorption of its material. The element with the maximum internal energy was always at the root of an impacted blade.

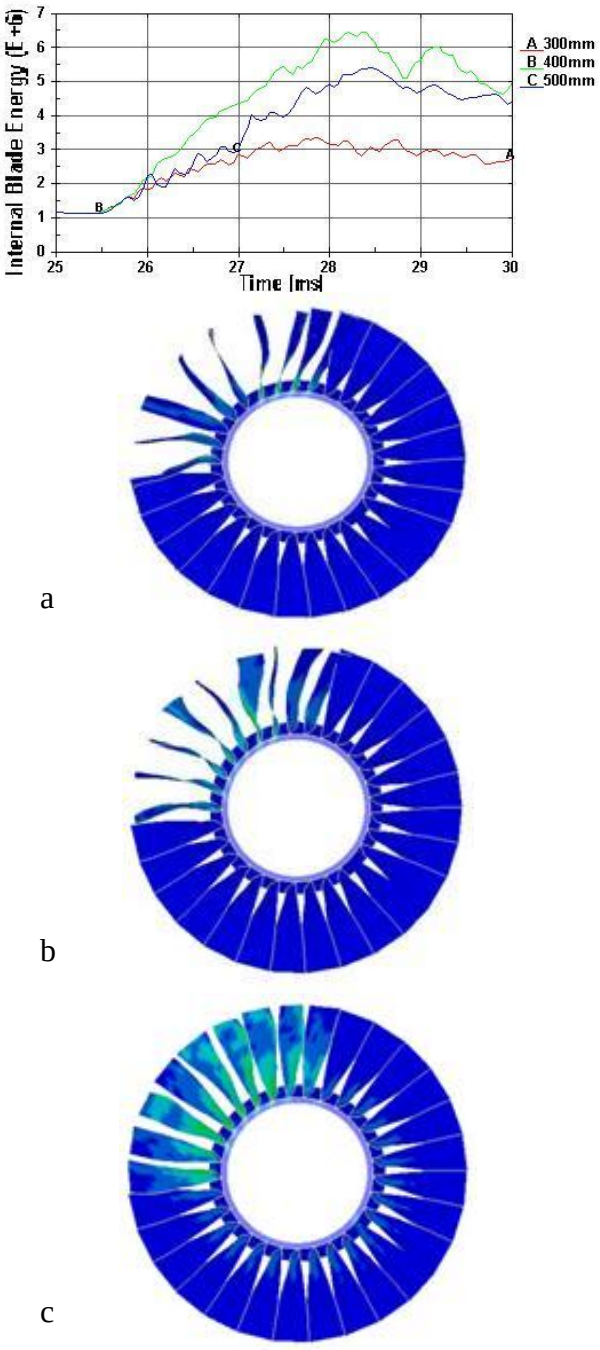

Fig. 17. Graph and illustrations showing the energy absorbed by the blade along the three positions studied. Post impacts at a)500mm b)400mm and c)300mm are shown

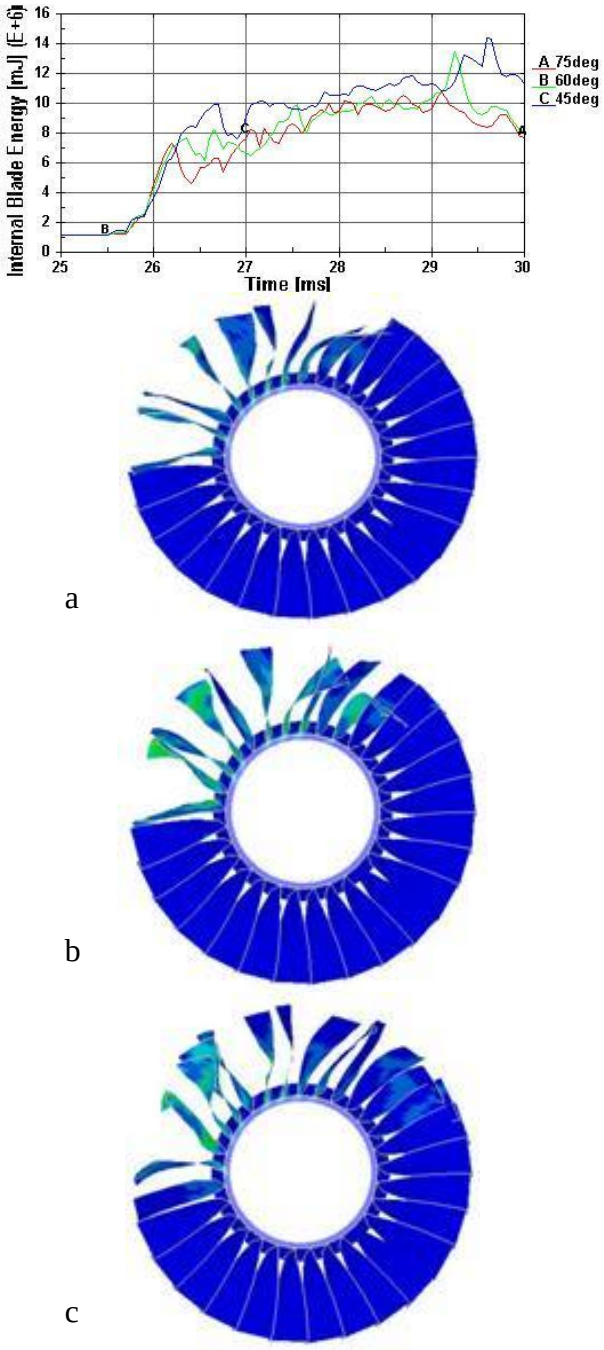

Fig. 18. Graph and illustrations showing the energy absorbed by the blade along three angles studied at 500mm of the span. Post impacts at a)75^0 b)60^0 and c)45^0 are shown

From Fig. 17 the most vulnerable location along the span was at 400mm from centre of rotation. This is due to a number of factors such as the relative speed and angle of attack of the bird, and the variation of internal and kinetic energy along the span of the blade.

The most damaging angle of impact investigated was at 45^0 as shown in Fig. 18. The 90^0 case is shown in Fig. 17. This is due to a combination of the higher relative velocity and angle of attack. It will later be shown that if the angle of attack is low, then little damage is sustained by the blades. Also, since the vertical velocity component was relatively lower, the

bird lingered in the impact region for longer thus increasing the number of blades damaged.

The SPH particles exhibit fluid like behaviour when impacting as expected. The majority of the particles are centrifuged away from the axis of rotation as expected. However, a few stray particles are thrown in random directions due to particles moving outside of two smoothing lengths of neighbour particles.

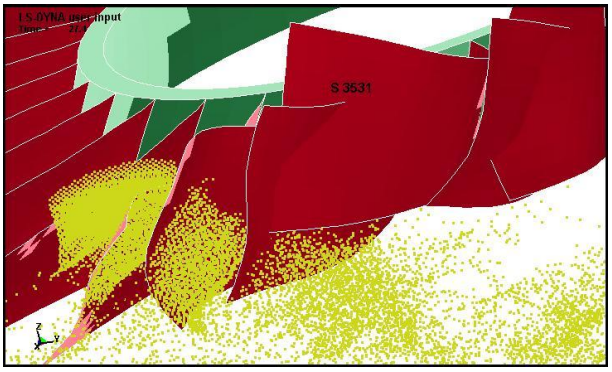

Fig. 19. Bird material being collected for impact on a fan with no blade contacts, TSSFAC=0.9, at 500mm span and 90^0 impact angle.

The results indicate that bird material is collected by the blades (Fig. 19), however, below a 'critical' angle of attack the bird is sliced (Fig. 20). Finding the critical angle was beyond the scope of this paper, however, it is expected to vary for different blade cross-sections; analogous to the flow behaviour over an aerofoil. When the bird is sliced at low angles of attack, the damage received by the blade is less [3]. This can be seen by comparing the internal energy histories from Fig. 17, Fig. 18 and Fig. 21.

Fig. 20. Post-Impact of the bird after it struck the blades at approximately zero angle of attack.

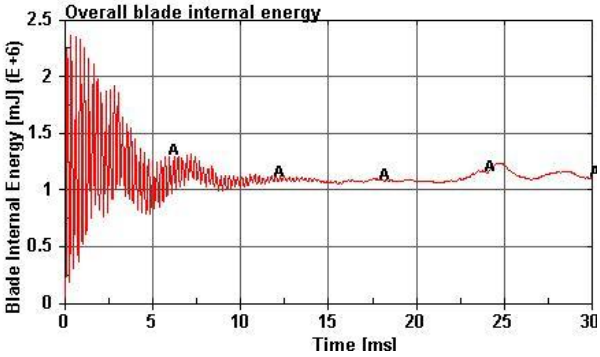

Fig. 21. Internal energy plot of the fan impacted at zero angle of attack.

The TSSFAC made a large impact in the results as shown in Table 3 and thus should be considered when utilizing SPH techniques. The number of blades damaged in either case was the same, however the maximum internal energies were higher when the time-step was halved; sometimes by up to 60.4% as for the 45 degree impact case. The maximum local energy appears less predictable with most cases sustaining more damage. However a few cases showed that although the maximum internal energy was higher, the maximum local energy was lower.

Table 3. Comparison between the two TSSFACs examined

γ [deg]	r [mm]	Max Internal Energy (kJ) TSSFAC 0.9	Max Internal Energy (kJ) TSSFAC 0.45	Max local energy (mJ/mm^3) TSSFAC 0.9	Max local energy (mJ/mm^3) TSSFAC 0.45
90	300	3.4	3.5	162.1	140.7
90	400	6.5	8.3	271.8	467.0
90	500	5.4	6	292.9	283.7
75	500	10.8	15.5	1113.8	1245.7
60	500	13.5	16.4	1522.0	1643.8
45	500	14.4	23.1	1928.3	2405.7

It was found that halving the time-step doubles the simulation time. One way of reducing this effect is to initialize the loads in the blade using TSSFAC=0.9 and then performing a restart analysis with the bird model and TSSFAC=0.45.

The ALE and SPH techniques exhibited differences as well as similarities. The

differences were as follows (refer to Table 5) for numerical results:

Numerical differences. The ALE technique always produced higher maximum internal energies than the SPH technique as shown in Table 5. However, when the SPH has TSSFAC=0.45, the SPH technique predicts higher maximum local damage for angled impactors.

Fluid-solid interactions. The ALE technique exhibited no penetrations, whereas a few SPH particles appeared to penetrate the blades. However, the particles that did not penetrate the blades showed similar fluid-solid interactions as the ALE technique.

Simulation times (Table 4). When comparing SPH and ALE for the same TSSFAC, The computational speed depends on the amount of deformation underwent by the impactor. Table 4 shows that SPH was faster for the angled impacts, which also incurred considerably more 'damage' in both techniques, as depicted in Table 5. This may be an issue when simulating impact on later stages of the engine as the impactor deformation will increase with subsequent impacts. However, as the time-step had to be reduced for the SPH technique, all simulations were lengthier than the ALE technique.

Table 4. Simulation times in seconds

		SPH		ALE
		TSSFAC		TSSFAC
γ [deg]	r [mm]	0.9	0.45	0.9
90	300	1642	3290	1583
90	400	1625	3290	1413
90	500	1593	3321	1589
75	500	1809	3408	2491
60	500	1750	3511	2874
45	500	1969	3448	2909

The ranking of damage per blade is slightly different as shown in Table 5.

There were many similarities observed as follows:

The bird behaviour observed was similar. Both the ALE and SPH cases showed the bird being thrown outwards, and breaking up in a similar fashion. It was observed that the blades 'climbed' through the bird in both cases.

The ranking of most to least damage was the same in each overall damage case. As observed in Table 5, the most damaging case was the 45^0 angle of impact and the least damaging was the impact at 300mm from the centre of rotation.

Most damage occurred at the root compared to the point of impact. All of the elements that sustained the highest internal energies were located at the root.

The statistics in Table 5 show moderate variation. This shows that with careful calibration, the results can be made to be more similar.

The slope in Fig. 22 is initially the same for the ALE and SPH impacts. This may be due to the fact that both have the same bulk modulus. However, the SPH particles appear to break apart more readily, as the damage steadily increases after the initial impact. The ALE method causes most of its damage at the time of impact with the internal energy slowly decreasing after the peak.

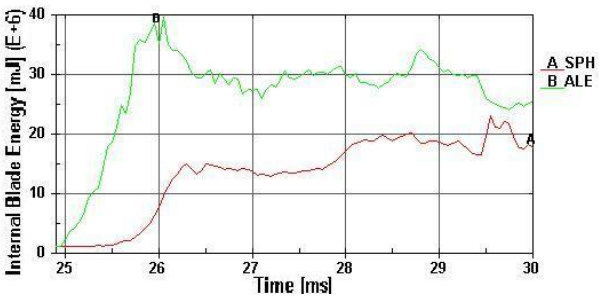

Fig. 22. Overall energy-time histories for the ALE and SPH technique (TSSFAC=0.45, no blade-to-blade contacts) with the impactor angled at 45^0

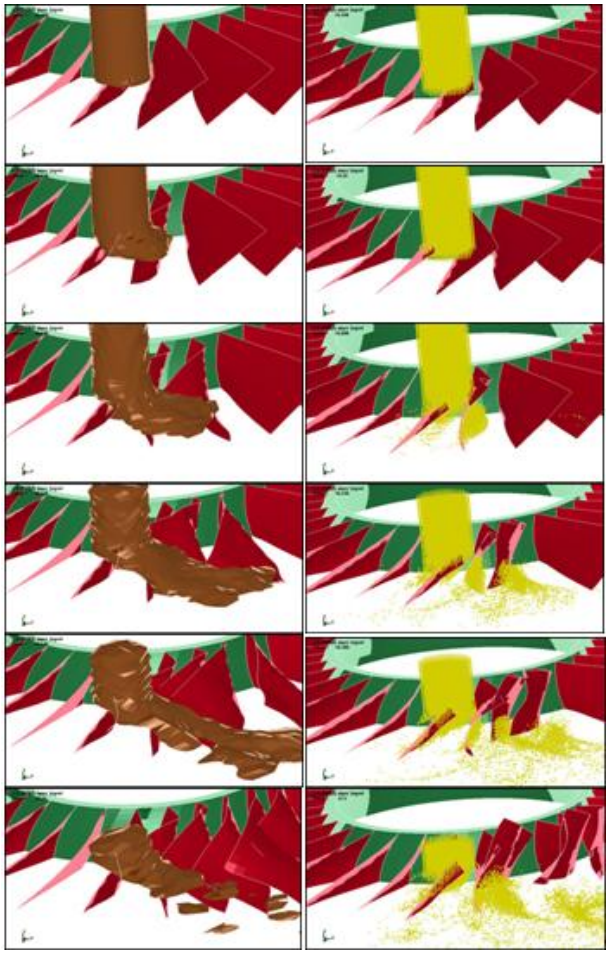

Fig. 23. Progressive damage of the ALE bird (left) impacting the blade at 500mm and 90^0 compared to the SPH bird (left) impacting in the same case.

Compared to the impact on the rigid plate (Fig. 4), the difference is large. This is due to the additional sources of error introduced when replacing the rigid plate with a fan. The sources of error include:

Difference in ALE medium compared to SPH medium. The ALE bird represents a continuous medium, whereas the SPH represents particles with empty space between them. This is especially important when the bird impacts the edge of the blade as the surface area of the edge is relatively small compared to the rigid flat plate. This has implications for the SPH technique as the results can vary depending on the percentage of void that is impacted compared to SPH particles. In addition, the results suggest that the positioning of particles may have an impact on the amount of local damage incurred. This is illustrated in Fig. 24 where the particles in geometry b) will collapse in between neighbour particles in contrast to geometry a) if they impacted the target at right angles. The ALE technique is not sensitive to this phenomenon.

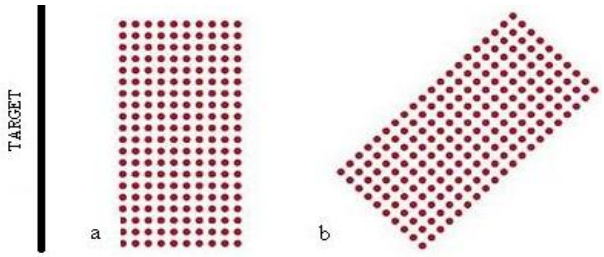

Fig. 24. Geometry a) ($\gamma=90^0$) will impact the target with a different particle arrangement compared to geometry b) ($\gamma=45^0$)

SPH particle edge geometry compared to the ALE element edge geometry. The ALE bird has a continuous surface compared to the rounded SPH bird particles.

Complex blade geometry. Compared to a flat plate, the blade is curved non-linearly in the x, y and z directions. In addition the bird is impacting on the edge of these curvatures

The nature of the blade material and fan rotation. The fan was modelled with deformable materials compared to a rigid plate. Therefore, compared to when the SPH bird-strikes, the ALE bird causes the geometry to deform sooner, thus causing it to impact a different geometry at a given time t after impact.

Difference in fluid behaviour. As shown in Fig. 9, the shape of the force-time histories were quite different, including when the SPH particle density was increased eight fold. The increase in particle density decreased the difference in medium and bird geometry errors which were not present in the ALE model. Thus, the SPH solution was expected to approach that of the ALE solution.

The fans with blade-to-blade contacts followed similar patterns to the fans without contacts. However, they received less damage in terms of local and overall energies but incurred a larger number of blades damaged. This was expected as for a given impact energy, the blades 'bouncing' off each other distribute the energy across more blades. In addition, each time a blade rebounds, built up internal energy gets converted back into kinetic energy, thus lowering the overall internal energy.

Table 5. A comparison between the SPH and ALE results for the fan with no contacts between blades. The SPH simulations where the TSSFAC=0.45 are being compared. The percentage difference column shows the calculated difference between the ALE and SPH overall damage solutions.

Angular Velocity	7300 RPM	**Blades internal energy from impact**				
Bird Speed	103m/s	**Overall Damage ALE [kJ]**	**Maximum Local Damage ALE [mJ/mm^3]**	**Overall Damage SPH [kJ]**	**Maximum Local Damage SPH [mJ/mm^3]**	**Difference (overall damage) %**
Span	300mm	6.5	423.096	3.4	140.659	47.7
	400mm	17.6	804.587	8.1	467.035	53.4
	500mm	13.6	427.722	5.9	283.671	55.9
Angle of Incidence (deg)	75	24.1	1197	15.4	1245.73	36.0
	60	28.3	1194.9	16.3	1643.75	42.4
	45	39.6	1302.74	23.0	2405.67	41.8
Mean difference	46.2%	**Standard Deviation**	7.6%	**Coefficient of Variation**	16.4%	

6 Conclusion

Metallic and composite single blades have been successfully modelled with aerodynamic, centrifugal and impact loading as well as a full metallic fan with centrifugal and impact loading. In all models, shells have been used for the blades, and restraints applied to a rigid hub. SPH and ALE techniques have been used to model the bird.

It was necessary to pre-stress the blade models before impact. Dynamic relaxation is a method of achieving this, however, as shells were used, the method is more time consuming compared to if it were used on solids. In addition, simply ramping up the loads in the blades provides a more robust solution, as it is not necessary to define a "dynamic relaxation factor"

The SPH method appears to be a suitable method for modelling the fluid behaviour of the bird. It captures the shock and release conditions described by ref. [11] for different angles and locations along the blade span. It is recommended to reduce the time-step when using the SPH technique. Failure to do so can result in particle penetration and a large variation in solutions. Halving the time-step appears appropriate, however a parametric study and experimental results are needed to verify the most suitable magnitude of reduction.

When impacting a rigid flat target, the ALE and SPH methods produced similar solutions, with ALE slightly over-predicting compared to SPH. However, when the rigid target is replaced by a blade, the differences become apparent. The SPH technique displayed more peaks than the ALE technique in the force-time histories, with a higher maximum peak force. Refining the SPH particle density caused more pronounced peaks, suggesting that the difference between the two techniques is more numeric than because of the void between SPH particles. Although the SPH bird produced higher peak forces on the blade, The ALE bird delivered the highest impulse into the blade, causing the most damage.

Impacts onto the rotating fan again revealed that ALE was more damaging to the fan. However, the fluid behaviour over the impactor was quite similar for the range of impact angles and locations along the span investigated. Additionally, as the time-step had to be reduced for the SPH models, the SPH solutions were more computationally expensive. However, when using SPH, the simulation time is independent of impactor distortion, whereas, the simulation time tended to increase for the more severely deformed ALE impactors. This may be an issue when simulating impact on later stages of the engine as the impactor

deformation will increase with subsequent impacts.

The positioning of SPH particles in the bird affects the results. This may need to be considered when simulating impact at different angles of attack

The Chang-Chang failure criteria appears to be suitable for high speed impact as in this case. It displays catastrophic crack propagation through the structure and captures various failure modes. The composite solutions displayed damage before impact which could be due to the lack of integration points used.

The two phase, ramp-up and restart method developed for creating the composite blade has many advantages. Firstly, it is a robust method that can be used for any fan. Secondly, it is expected that a fast ramp-up can take place with unrealistically high failure criteria, which can then be set to normal for the second phase of the analysis. Thirdly, particularly for the SPH technique, the time-step can be as per usual for the first phase, and then reduced for the impact phase. Lastly, it is a flexible technique that allows the user to ramp up the model once and then make minor adjustments or analyse different impact scenarios, such as flock encounters, different impact angles, different bird geometries, etc, all starting from the second phase.

It is expected that a similar method can be applied to a full rotating composite fan. The first phase will likely be the same as for the blade. The body load will likely be used rather than assigning a prescribed velocity to the hub as in ref [10], as the sudden hub ramp up will concentrate stresses at the root rather than distribute them across the blade. The second phase is expected to be completed by removing the body load and assigning a rotational velocity to the blades and a constant prescribed motion to the hub. The hub rotational axis degree of freedom will also need to be freed. Finally, a bird will need to be added to the model and assigned an initial velocity.

7 Future Work

As well as creating a composite fan model, the following work is planned:

- Advancing the assumptions in the aerodynamic load analysis
- Adding aerodynamic loads to a fan
- Further investigation into the fluid-solid interactions of the SPH and ALE techniques and comparing them to experimental results. In addition use of friction in the analysis is intended.
- Investigation into various impactor geometries to find which is most suitable for impact of the most common bird species
- Modelling the fan without a fixed centre of rotation to investigate the effect of vibration induced due to mass lost or shifted about the rotational axis.
- Investigation into different types of composite materials, for example metallic foam core composites [12], Titanium matrix composites [13] and fabric reinforced composites. Further investigation into carbon fibre reinforced composites is also planned.

8 Acknowledgements

The authors would like to acknowledge Prof. Bayandor's Team for their constructive feedbacks throughout this research program.

9 References

[1]. Wilbeck, J S and Barber, J P, Bird Impact Loading. *The Shock and Vibration Bulletin*, Vol.48 Part 2, pp115-112, 1978

[2]. Bayandor, J, et al. *Impact Damge modelling of composite aerospace structures subject to bird strike*. in *25th International Congress of the Aeronautical Sciences*. Melbourne 2006.

[3]. Huertos-Ortecho, C, *Robust Bird Strike Modeling Using LS-DYNA*, University of Puerto Rico 2006

[4]. Tata, D, *Impact damage modelling in advanced aerospace composite structures subject to bird strike*, School of Aerospace Mechanical and Manufacturing Engineering., RMIT University ; 2006

[5]. Monaghan, J J, An introduction to SPH. *Computer Physics Communications*, Vol.48, No.1, 89-96, 1988

[6]. Jenq, S T, et al., Simulation of a rigid plate hit by a cylindrical hemi-spherical tip-ended soft

impactor. *Computational Materials Science*, Vol. in Press, Corrected Proof,

[7]. Kim, M K, *Investigation and modelling of soft body impact onto jet engine composite fan*, Undergraduate Degree School of Aerospace Mechanical and Manufacturing Engineering RMIT University 2007

[8]. Zammit, A, *Bird-strike Damage Analysis in Concept Advanced Composite Fan Blades using Smoothed Particle Hydrodynamics*, Final Thesis, School of Aerospace, Mechanical and Manufacturing Engineering RMIT 2007

[9]. Hallquist, J O, *LS-DYNA Theory manual*. 2006, Livermore Software Technology Corporation: Livermore, California.

[10]. Shultz, C and Peters, J, *Bird Strike Simulation Using ANSYS LS/DYNA*. 2002, Phoenix Analysis and Design Technologies, Inc.

[11]. Wilbeck, J S, *Impact Behavior of Low Strength Projectiles*. 1978, Air Force Materials Laboratory: Ohio.

[12]. Ghosn, L J, et al. *Evaluation of a 17-4 PH stainless steel sandwiched fan blade design concept*. Pittsburgh, PA, United States Vol.3 21-32 2005.

[13]. Leyens, C, et al., Materials and design concepts for high performance compressor components. *Aerospace Science and Technology*, Vol.7, No.3, 201-210, 2003

10 Copyright Statement